# Effect of H, He and Ar irradiation on β-$Ga_2O_3$ material

S. X. Sun[a,b,c,*], Y. Z. Wu[b], H. Y. Mei[d]
[a]*Chongqing Institute of Microelectronics Industry Technology, University of Electronic Science and Technology of China, Chongqing 401331, China*
[b] *College of International Education, Shenyang University, Shenyang 110044, Chna*
[c]*School of Electronic Science and Engineering, University of Electronic Science and Technology of China, Chengdu 610054, China*
[d]*Henan Key Laboratory of Smart Lighting and School of Electronic Information, Huanghuai University, Zhumadian 463000, China*

In this work, the projected range, the nuclear stopping power(Sn), electronic stopping power (Se), vacancies, replacement collisions, and total target damage of β-$Ga_2O_3$ by H, He and Ar ion bombardment are investigated by the Monte Carlo SRIM software. The ions were vertically incident on a 1-um β-Ga2O3 material, and their energies varied from 100 keV to 1 MeV. The results showed that the projected range increased for all three ions with increasing incident energies, with H ions having the largest projected range. The Sn for Se with incident energy of 0-1MeV in β-$Ga_2O_3$ is much greater than the Sn for H and He, while the Sn for Ar decreases gradually with the increase of incident ion energy, and the Se shows a gradual increasing trend. Compared with H and He, the number of vacancies induced by Ar were the largest at the same incident energy and thickness of β-$Ga_2O_3$. In addition, it is obvious that the total target damage of Ar on β-$Ga_2O_3$ material were much more serious than H and He.

(Received February 19, 2023; Accepted May 2, 2023)

*Keywords:* β-$Ga_2O_3$, Particle irradiation, Stopping power, Total target damage

## 1. Introduction

With the development of science and technology, society has gradually increased its requirements for materials[1]. The properties of the first and second generation of semiconductor materials have reached their theoretical limit, greatly limiting their application in the fields of high temperature, high frequency, and high power devices[2].

As an excellent semiconductor material, β-$Ga_2O_3$ has many advantages such as a wide bandgap, high breakdown voltage, good radiation resistance, chemical stability, and thermal stability[3-5]. As an emerging ultra-wide bandgap semiconductor material, it has a bright prospect in various fields such as radiation detection, aerospace, integrated circuits, medical treatment, and new energy, making it a material with great research potential[6,7].

* Corresponding author: sunshuxianga@126.com
https://doi.org/10.15251/DJNB.2023.182.557

Due to the excellent performance of β-$Ga_2O_3$-based electronic devices in harsh environments, gallium oxide has been extensively used in deep ultraviolet detection and other fields, particularly in various areas of optical exploration, especially in spacecrafts[8-11]. When high-energy particles penetrate the material, point defects or defect clusters occur, affecting its physical properties and further impacting the device's performance indicators[12]. Thus, understanding the stability mechanism of gallium oxide defects is crucial for the development of reliable devices and circuits in space missions and nuclear facilities.

At present, with the advancement of β-$Ga_2O_3$ single crystal and semiconductor device preparation technology, research on the radiation damage effect of β-$Ga_2O_3$ materials and devices for space applications is also underway. Studies have been conducted on the ion irradiation effects of β-$Ga_2O_3$ materials and devices[13-15], and it has been found that the radiation resistance of β-$Ga_2O_3$ materials and devices is comparable to that of GaN in environments where neutrons, protons, and heavy ions are mainly damaged by elastic collisions with target atoms. This indicates that β-$Ga_2O_3$ has excellent radiation resistance and great potential for future applications in the aerospace field[16]. However, compared to SiC and GaN, research on the radiation damage properties of β-$Ga_2O_3$ materials and devices is still in its early stages, and there are relatively few research results.

This study investigated the behavior of ion range, electronic stopping power, nuclear stopping power, vacancies, replacement collisions, and energy loss of β-$Ga_2O_3$ induced by H, He, Ar, and Ta using the SRIM-2013 software. The ion energy was ranged from 100 keV to 1 MeV. This research will help to explore the radiation damage effect and mechanism of semiconductor materials and devices, providing a basis for the application of devices and circuits in space environments and for improving the irradiation hardening technology.

## 2. Simulations

In this work, the SRIM software was used to research the irradiation effects on β-$Ga_2O_3$ material. The collision between the incident particle and the target nucleus of the material is described by two-body collision[17]. The software includes SRIM and TRIM. In this study, projected range, the nuclear stopping power(Sn) and electronic stopping power (Se) were calculated by SRIM. The recoil of atoms, vacancies, energy loss (%) can be obtained by the TRIM program[18].

The incident energy of ions were ranged from 100 keV to 1 MeV with the vertically direction. The thickness of β-$Ga_2O_3$ was set as 1 um. In the simulation, the density of material and the threshold displacement energies were most important parameters. In this paper, the density of β-$Ga_2O_3$ was set as 5.88 g/$cm^3$, and the threshold displacement energy for Ga and O were set as 25 eV and 28 eV[19], respectively. The total number of incident particle was set $10^4$ in each simulation[20] and well avoided higher fuctuations and to obtain better statistical values. The “Detailed Calculation with full Damage Cascades” mode was selected.

## 3. Results and discussion

Radiation damage zone is an important aspect of material radiation effect research. The radiation damage zone can be directly reflected by the projected range in the direction of the incident ion. After multiple collisions with the nucleus and extra-nuclear electrons of the material, the average distance between the starting and ending position of the ion in the material is known as the projected range. Figure 1 illustrates the range of three different ions as a function of energy in β-$Ga_2O_3$ material. As can be seen from the figure, the projected range of the three ions in β-$Ga_2O_3$ increases with the increase in incident energy. However, the projected range of hydrogen in β-$Ga_2O_3$ is much greater than that of helium and argon. This is mainly due to hydrogen having the smallest atomic number, which means it has a small mass and will have a greater velocity under the same incident energy[21]. As a result, the probability of collision with gallium and oxygen during the incident process is less than with helium and argon, and the energy loss per unit range is small, leading to hydrogen reaching deeper into the β-$Ga_2O_3$. Therefore, the damage zone is further away from the β-$Ga_2O_3$ surface for small atomic number ions at the same incident energy.

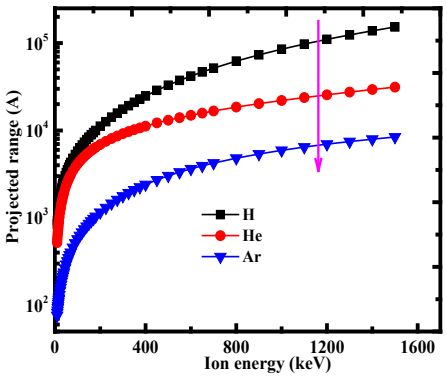


*Fig. 1. Projected ranges of H, He and Ar in β-$Ga_2O_3$ with different incident energies.*

Figure 2(a) and (b) show the longitudinal and lateral straggling of β-$Ga_2O_3$ for interactions with H, He, and Ar, respectively.

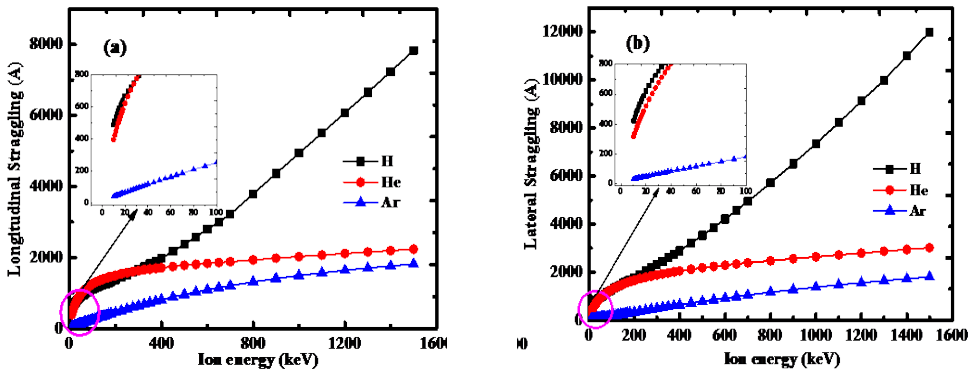


*Fig. 2. Longitudinal and lateral straggling of the β-$Ga_2O_3$ for H, He and Ar.*

It is seen from the figures that H has the highest straggling values at lower and higher energies for β-$Ga_2O_3$, respectively, while Ar has the lowest values at lower and higher energies for β-$Ga_2O_3$, respectively. H has a relatively light mass, and its incidence direction is greatly changed due to the scattering effect of atoms after incident[22], lead to the large longitudinal and lateral distribution in β-$Ga_2O_3$. However, for He and Ar with large mass, the direction of incident ions does not change much after interaction with atoms, and their longitudinal and lateral distribution in β-$Ga_2O_3$ is relatively small.

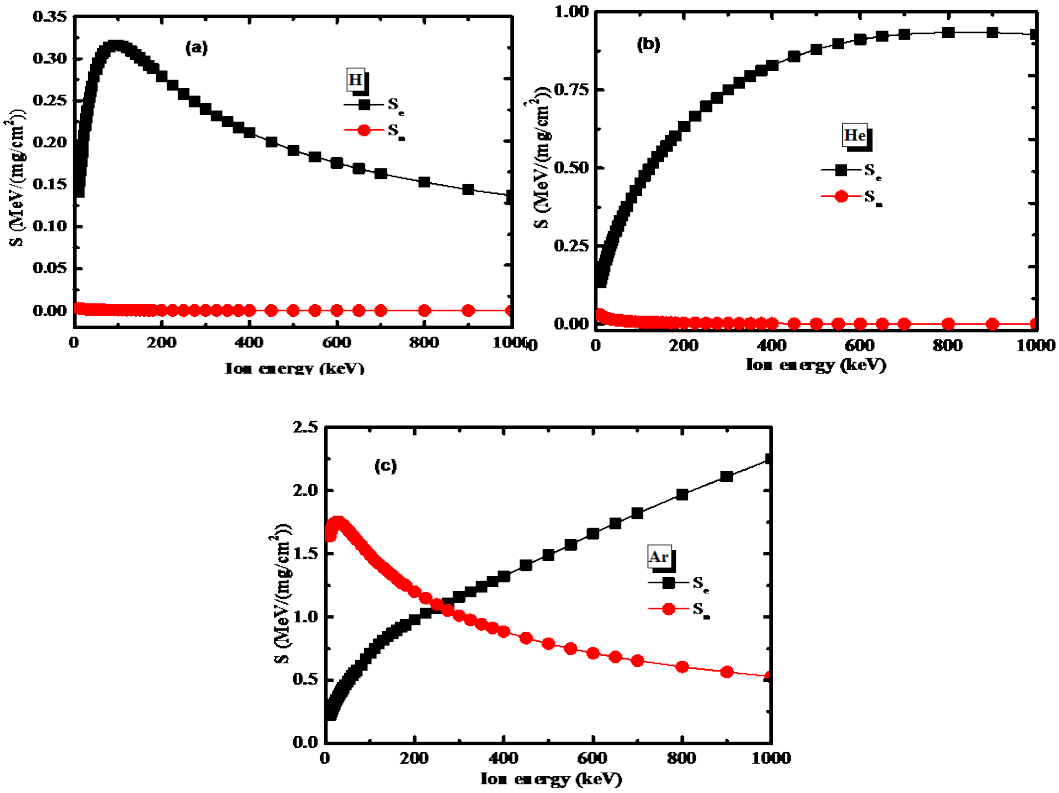


*Fig. 3. Electronic stopping power (Se) and nuclear stopping power (Sn) for (a) H, (b) He and (c) Ar with target of β-$Ga_2O_3$ versus incident ion energy.*

In order to analyze the type of radiation damage, the stopping power of β-$Ga_2O_3$ was calculated. The stopping power can be described by the energy loss of the incident ion per unit path, reflecting the stopping power of the atoms and extranuclear electrons of β-$Ga_2O_3$ on the incident ion. Figure 3 (a), (b), and (c) show the nuclear stopping power (Sn) and electron stopping power (Se) of H, He, and Ar in 1um β-$Ga_2O_3$, respectively, for incident energy ranging from 0 to 1 MeV. As shown in Fig. 3 (a) and (b), at energies ranging from 0 to 1 MeV, the Sn of H particles increases first and then decreases, while for He, the Sn first increases and then tends to remain unchanged. However, the Se with an incident energy ranging from 0 to 1 MeV in β-$Ga_2O_3$ is much greater than the Sn for H and He, meaning that the energy loss of H and He ions is mainly due to electron energy loss, and the irradiation damage effect is mainly due to ionization. As seen in Fig. 3 (c), the Sn for Ar decreases gradually with an increase in incident ion energy, while the Se shows a gradual increase. When the incident ion energy ranges from 0 to 260 keV, the Sn is greater than

the Se, indicating that the radiation damage effect is mainly due to displacement. When the incident energy ranges from 260 keV to 1 MeV, the Se is greater than the Sn, meaning that the radiation damage effect is mainly due to ionization. When the incident energy is ranged from 260 keV to 1 MeV, the $S_e$ is greater than the $S_n$, and the radiation damage effect is mainly displacement effect.

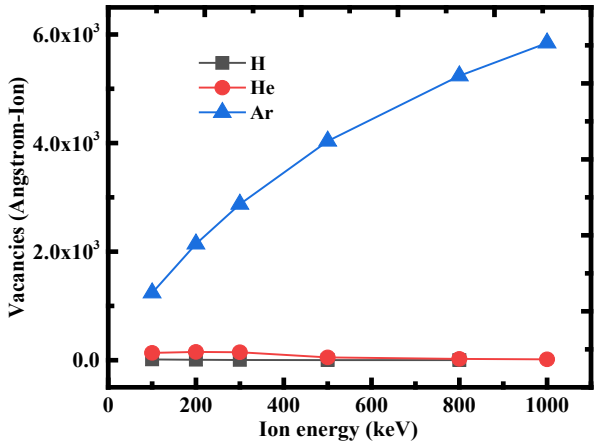


*Fig. 4. Vacancies created in β-$Ga_2O_3$ s by H, He and Ar bombardment as a function of the incident ion energy*

The number of vacancies is an essential physical parameter. Vacancies defects will be produced when an incident particle strikes the lattice position of the target atom. These defects induced by ion will change the electrical and mechanical characteristics of β-$Ga_2O_3$. Figure 4 shows the vacancies as a function of incident energy of H, He and Ar. It can be concluded that the number of vacancies produced by H and He decreases with increasing energy, while for Ar particles, the number of vacancies increases with increasing energy in the 1 um thickness of β-$Ga_2O_3$. When the energy is 1MeV, the number of vacancies generated by H and He is almost 0, while the number of vacancies generated by Ar reaches 5847. This is mainly due to the He ion is heavier than the H ion, and movement speed of He ion is smaller in the material, increases the chance of a collision with the target atom which led to creating more vacancies. At the same incident energy, H and He have higher velocities. High energy H and He are close to a straight line in their path of motion due to their high velocities[23], and only collide with a few lattice atoms, transferring little energy to lattice atoms and thus generating few vacancies. Figure 5-7 show the distribution of H, He and Ar in 1um β-$Ga_2O_3$ with different energies. The results show that the energy of H particle is more than 500keV, H particle has already penetrated β-$Ga_2O_3$, and for He particle, when the incident amount is larger than 1MeV, β-$Ga_2O_3$ has also penetrated. Therefore, with the increase of energy, the number of vacancies of H and He in the 1 um β-$Ga_2O_3$ decreases. As can be seen from Fig. 7, with the increase of Ar incident energy, the distribution of Ar ions becomes larger and larger. Therefore, with the increase of incident energy, the probability of ion displacement in the lattice when Ar collides increases, thus increasing the number of vacancies.

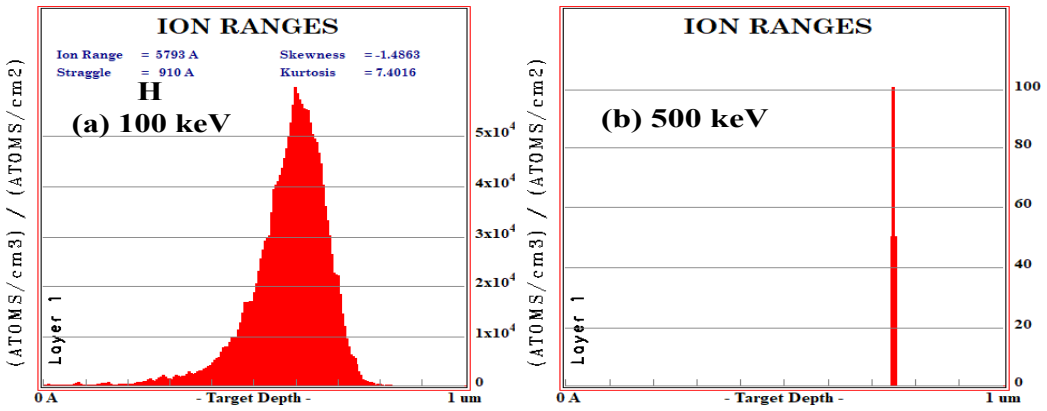


*Fig. 5. Distribution of H in β-$Ga_2O_3$ with different energies,(a) 100 keV, (b) 500 keV.*

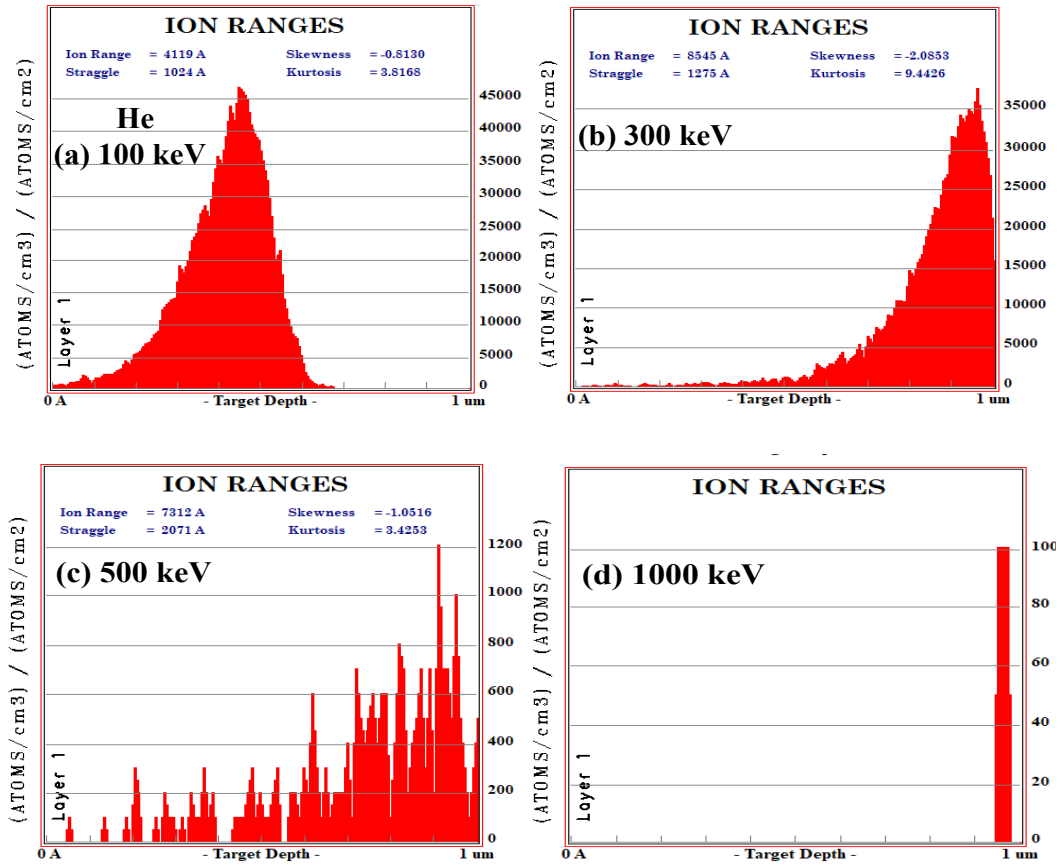


*Fig. 6. Distribution of He in β-$Ga_2O_3$ with different energies,(a) 100 keV, (b) 300 keV, (c) 500 keV, (d) 1000 keV.*

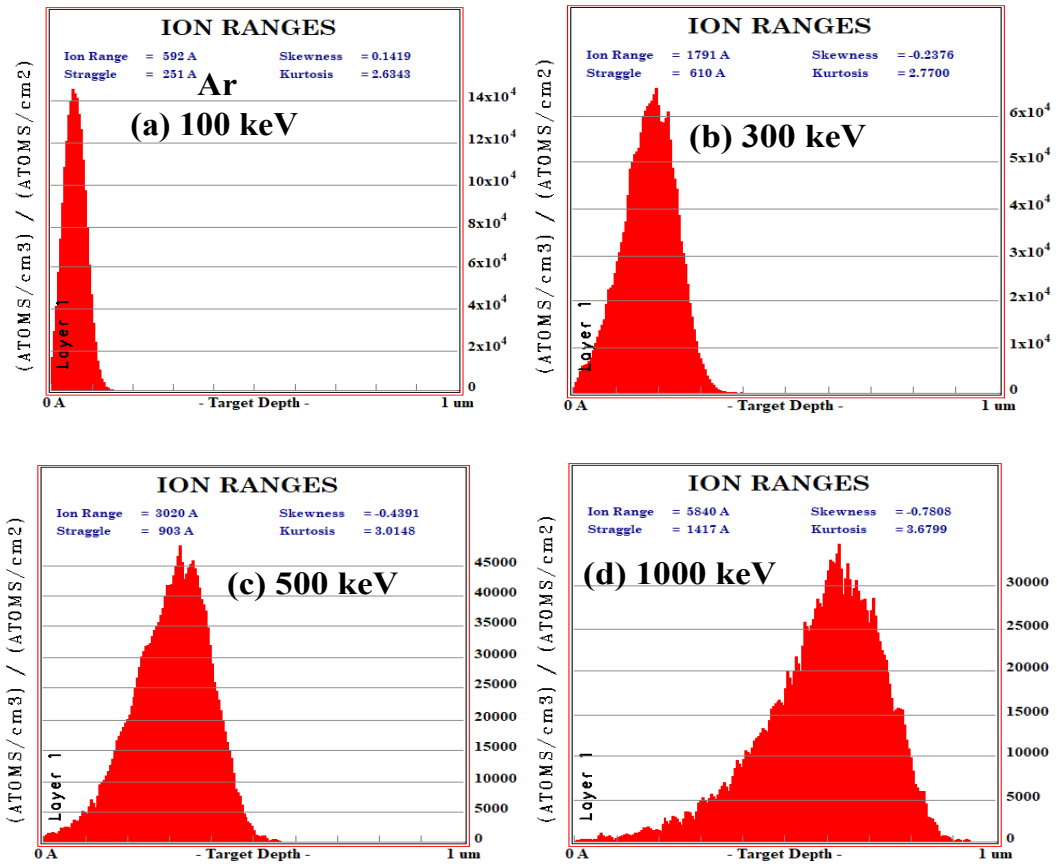


*Fig. 7. Distribution of Ar in β-$Ga_2O_3$ with different energies,(a) 100 keV, (b) 300 keV, (c) 500 keV, (d) 1000 keV.*

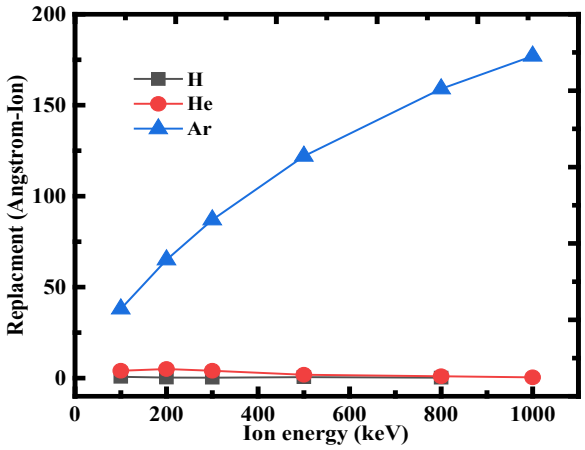


*Fig. 8. Replacements in β-$Ga_2O_3$ by H, He and Ar bombardment as a function of the incident ion energy.*

The total target damage, which is equal to the sum of the number of vacancies and replacement collisions, is a notable parameter when studying irradiation damage. Figure 8 shows the variation of replacement collisions induced by H, He, and Ar in β-$Ga_2O_3$ with different

incident energies. The trends of H, He, and Ar are similar to the variation of vacancies with increasing incident energy. Specifically, the number of replacement collisions for H and He decreases with increasing incident energy, while for Ar, the number of replacement collisions increases with increasing incident energy. The total target damage induced by H, He, and Ar in β-$Ga_2O_3$ is shown in Figure 9. As seen in Figure 9, the total target damage increases monotonically with the incident energy of Ar, and the values of total target damage are greater than those of total target damage induced by H and He. Therefore, irradiation of atoms with high atomic numbers causes greater damage.

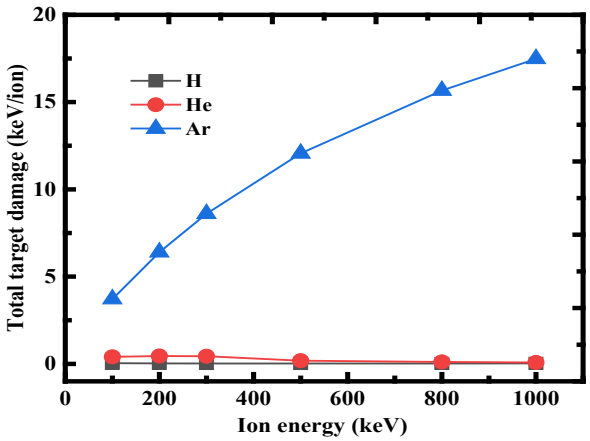


*Fig. 9. Replacements in β-$Ga_2O_3$ by H, He and Ar bombardment as a function of the incident ion energy.*

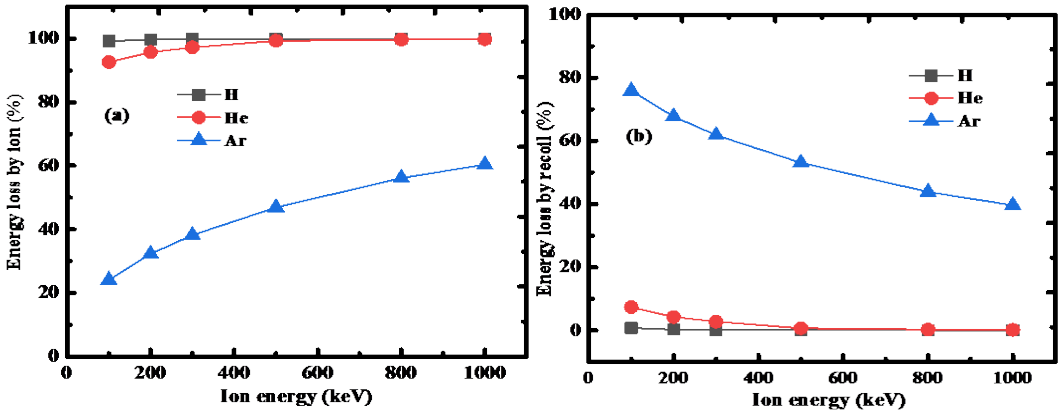


*Fig. 10. Energy loss (%) due to (a) ion and (b)recoil by H, He and Ar bombardment as a function of the incident ion energy.*

Figure 10 shows the variation of energy loss (%) due to ion and recoil with different incident energy for H, He and Ar in 1 um β-$Ga_2O_3$. It is observed that most of the energy loss is caused by the ion is increased with the increase of incident energy for H and He. The energy loss is caused by the recoil is decreased with the increase of incident energy for H and He. However,

when the energy exceeds 500 keV, the energy loss due to ion and recoil hardly changes for H and He. For Ar, with the increase of incident energy, the energy loss caused by ion gradually increases, while the energy loss caused by recoil gradually decreases. Therefore, particles with large atomic number have a greater influence on the β-$Ga_2O_3$ material properties at a certain thickness.

## 4. Conclusions

In summary, the effects of H, He, and Ar irradiation with different energies on β-$G_2O_3$ were investigated through numerical simulation. The results showed that the projected range of the three types of ions increases with increasing incidence energy, and the projected range of H is larger than that of He and Ar at all energies. H had the highest straggling values at lower and higher energies for β-$G_2O_3$, respectively, while Ar had the lowest values at lower and higher energies for β-$G_2O_3$, respectively. The SE with an incident energy of 0-1 MeV in β-$G_2O_3$ was much greater than the SN for H and He, indicating that the irradiation damage effect was mainly an ionization effect. For Ar, the radiation damage effect was mainly a displacement effect with 0-260 keV and mainly a displacement effect with 260 keV-1 MeV. The number of vacancies produced by H and He decreased with increasing energy, while for Ar particles, the number of vacancies increased with increasing energy in the 1 um thickness of β-$G_2O_3$. The total target damage increased monotonically with the incident energy of Ar, and the values of total target damage were larger than the value of total target damage induced by H and He. Therefore, irradiation of atoms with large atomic numbers causes greater damage.

**Acknowledgements**

This research was funded by the Key Scientific Research Projects of Colleges and Universities in Henan Province (No.22A510016), National Natural Science Foundation of China (No. 62204094), China Postdoctoral Science Foundation (No.2021M700685), Henan Provincial Science and Technology Research Project (No. 222102310286, 232102210173).

## References

[1] E .A. Jones, F. F. Wang, D. Costinett, IEEE Journal of Emerging and Selected Topics in Power Electronics 4, 707-719 (2016); https://doi.org/10.1109/JESTPE.2016.2582685

[2] B. Mounika, J. Ajayan, Sandip Bhattacharya, D. Nirmal, Micro and Nanostructures 168, 207317 (2022); https://doi.org/10.1016/j.micrna.2022.207317

[3] J. H. Choia, C. H. Chob, H. Y. Cha, Results in Physics 9, 1170-1171 (2018); https://doi.org/10.1016/j.rinp.2018.04.042

[4] D. H. Liu, Y. W. Huang, Z. Y. L. Zhang, D. Z. Chen, Q. Feng, H. L. You, J. C. Zhang, C. F. Zhang, Y. Hao, ECS Journal of Solid State Science and Technology 10,125001 (2021); https://doi.org/10.1149/2162-8777/ac3afd

[5] S. J. Pearton, J. Yang, P. H. Cary, F. Ren,J. Kim,M. J. Tadjer,M. A. Mastro, Appl. Phys. Rev. 5,

011301 (2018); https://doi.org/10.1063/1.5006941

[6] S. Baskaran, M. Shunmugathammal, C. Sivamani, S. Ravi, P. Murugapandiyan, N. Ramkumar, Silicon 14, 11079-11087 (2022); https://doi.org/10.1007/s12633-022-01846-w

[7] X. Chen, F. Ren, S. Gu, J. Ye, Photonics Research 7(4), 381 (2019); https://doi.org/10.1364/PRJ.7.000381

[8] M. I. Pintor-Monroy, B. L. Murillo-Borjas, M. A. Quevedo-Lopez, ACS Applied Materials & Interfaces 2, 3358-3365 (2020); https://doi.org/10.1021/acsaelm.0c00643

[9] B. R. Tak, R. Singh, ACS Applied Electronic Materials 3,2145-2151 (2021); https://doi.org/10.1021/acsaelm.1c00150

[10] R. D. Qiao, H. P. Zhang, S. T. Zhao, L. Yuan, R. X. Jia, B. Peng, Y. M. Zhang, Journal of Physics D: Applied Physics 55, 383003 (2022); https://doi.org/10.1088/1361-6463/ac7c44

[11] D. Guo, Q. Guo, Z. Chen, Z. Wu, P. Li, W. Tang, Materials Today Physics 11, 100157 (2019); https://doi.org/10.1016/j.mtphys.2019.100157

[12] N. Manikanthababu, H. Sheoran, P. Siddham, R. Singh, Crystals 12, 1009 (2022); https://doi.org/10.3390/cryst12071009

[13] G. Yang, S. Jang, F. Ren, S. J. Pearton, J. Kim, ACS Applied Materials & Interfaces 9, 40471-40476 (2017); https://doi.org/10.1021/acsami.7b13881

[14] W. S. Ai, L. J. Xu, S. Nan, P. F. Zhai, W. X. Li, Z. Z. Li, P. P. Hu1, J. Zeng, S. X. Zhang, L. Liu, Japanese Journal of Applied Physics 58, 120914 (2019); https://doi.org/10.7567/1347-4065/ab5599

[15] E. Farzana, M. F. Chaiken, T. E. Blue, A. R. Arehart, S. A. Ringel, APL Materials 7, 022502 (2019); https://doi.org/10.1063/1.5054606

[16] S. J. Pearton, A. Aitkaliyeva, M. Xian, F. Ren, A. Khachatrian, A. Ildefonso, Z. Islam, M. A. J. Rasel, A. Haque, A. Y. Polyakov, Ji. Kim, ECS Journal of Solid State Science and Technology 10, 055008 (2021); https://doi.org/10.1149/2162-8777/abfc23

[17] S. X. Sun , Y. H. Zhong, R. X. Yao, F. J. Cen, Y. X. Li, Digest Journal of Nanomaterials and Biostructures 15(4), 1089-1095 (2020).

[18] H. Y. Mei, S. H. Zhao, Y. Z. Wu, P. Zhang, H. T. Wu, R. X. Yao, X. Y. Zheng, H. Wen, S. X. Sun, Digest Journal of Nanomaterials and Biostructures 17(2), 749-758 (2022).

[19] P. Kachhawa, N. Chaturvedi, Surface and Interface Analysis 54, 1203-1210 (2022); https://doi.org/10.1002/sia.7145

[20] S. I. Radwan, M. M. Shehata, H. El-Khabeary, A. G. Helal, Radiation Physics and Chemistry 121, 93-98 (2016); https://doi.org/10.1016/j.radphyschem.2015.12.019

[21] H. Y. Mei, H. T. Wu, R. X. Yao, L. Y. Zhao, X. Y. Zheng, F. Liua, H. Wen , S. X. Sun, Digest Journal of Nanomaterials and Biostructures 17(1), 39-46 (2022).

[22] M. El Marsi, Z. Elmaddahi, I. Fechtal, A. Dezairi, Journal of Radioanalytical and Nuclear Chemistry 331, 3795-3806 (2022); https://doi.org/10.1007/s10967-022-08415-w

[23] M. Kurudirek, Nuclear Instruments and Methods in Physics Research A 795, 239-252 (2015); https://doi.org/10.1016/j.nima.2015.06.001